RNA-seq and cytological study of sex-specific meiosis response to Gsdf in medaka (Oryzias latipes)

Xi Li
Shanghai Ocean University
Xinwen Li
Shanghai Ocean University
Wenhao Li
Shanghai Ocean University
Yingqing Zhang
Shanghai Ocean University
Haiyan Guo
Shanghai Ocean University
Guangxing Wang
Shanghai Ocean University
Yayuan Li
Shanghai Ocean University
Xiaowen Wu
Shanghai Ocean University
Ruiqin Hu
Shanghai Ocean University
Siyu Wang
Shanghai Ocean University
Xiaomiao Zhao
Guangdong Academy of Medical Sciences
Liangbiao Chen
Shanghai Ocean University
Guijun Guan (gjguan@shou.edu.cn)
Shanghai Ocean University

Research Article

Keywords: BMP/TGFβ: Bone Morphogenetic Protein/Transforming Growth Factor beta, gsdf: gonadal soma-derived factor, synaptonemal complex proteins Sycp1, Sycp3, AS: RNA alternative splicing, SAC:

spindle assembly checkpoint

Posted Date: March 21st, 2022

DOI: https://doi.org/10.21203/rs.3.rs-1433778/v1

Abstract

Sexually dimorphic meiosis is monitored by meiotic recombination to prevent the formation of abnormal gametes in males and females. However, the regulatory mechanism of sex-specific meiotic recombination is not completely understood. Here we report the role of *gsdf*, a unique BMP/TGF-b family member gene, in the regulation of meiotic recombination in medaka (*Oryzias latipes*) based on the RNA-seq and cytogenetic analysis of normal and *gsdf* deficient gametogenesis. Several differentially expressed genes, including the FKB506-binding protein 7 (*fkbp7*), were significantly upregulated in pubertal *gsdf* deficient gonads. The escalation of alternative pre-mRNA isoforms of meiotic synaptonemal complex genes including *sycp3* were visualized using Integrative Genomics Viewer and confirmed by real-time qPCR. However, immunofluorescence analysis showed that Sycp3 protein products in *gsdf* deficient XY oocytes were significantly reduced. Transmission electron microscope observations showed that asynchronous cysts replaced normal synchronous cysts in *gsdf*-deficient testis. Breeding experiments revealed a skewed ratio of $gsdf^{-/-}$ XY gamete fertility in a non-Mendelian manner resulting in XY chromosome non-disjunction. Taken together, our observations suggest that Gsdf signaling may directly or indirectly affect meiotic recombination in the process of sex-specific division of germline stem cells.

Introduction

Male and female germ cells in vertebrates undergo different meiotic processes. Meiotic checkpoints strictly monitor these processes to prevent the formation of abnormal gametes (Hunt and Hassold, 2002). Germline stem cells (GSCs) are morphologically similar regardless of mitotic quiescence or activation after primordial germ cells (PGCs) reside in the genital ridge. Although the time courses of the sex-differentiated proliferation of GSCs vary among vertebrate species, male GSCs in testis usually arrest at the G0/G1 stage of the mitotic cell cycle, then undergo the progressive resumption of spermatogonia proliferation and meiotic differentiation to produce haploid spermatozoa. In contrast, most female GSCs enter meiosis and arrest at the end of the first meiotic prophase in the ovary during early oogenesis, forming a reserve of diplotene oocytes that are selectively recruited into follicular growth. Fully-grown oocytes resume the meiotic cell cycle and divide into haploid oocytes upon ovulation and fertilization after two cycles of polar body release (Gruhn et al., 2013). Cytological analysis has demonstrated the sex-specific differences in human meiotic recombination prior to the onset of double-strand breaks (DSBs) (Gruhn et al., 2013). Bone morphogenetic protein (BMP) signaling has been demonstrated to cooperate with retinoic acid (RA) to specify GSC female fate in mice (Miyauchi et al., 2017) and initiate meiosis through the upregulation of the female germline gene *Stra8*, while the male germline gene *Nanos2* downregulates *Stra8* (Sada et al., 2009). However, evidence of the normal meiosis of germ cells in mice that lack RA receptors suggests that RA may not be the pivotal factor (Vernet et al., 2008), but instead supports the feminizing effect of BMP alongside RA for germ cell sex specification (Miyauchi et al., 2017). In contrast to mammals, *Nanos2* is not the sexual fate marker in medaka (*Oryzias latipes*) germ cells, whereas *Stra8* is completely missing in medaka genomic databases (Nishimura and Tanaka, 2016).

Although the location of PGCs relative to somatic structure has been pre-established, the post-transcriptional regulation of specific mRNA expression patterns can directly affect the fate of GSCs in the process of sexual differentiation (Herpin et al., 2007). In addition, overexpressing BMP2 or a dominant negative form of the BMP2/4 receptor in medaka caused no change in the number of PGCs (Herpin et al., 2007). These results suggest that BMP signaling may have an indirect role in the sex fate determination of GSCs, although the entire mechanism remains to be elucidated.

The advantages of the identified *dmy/dmrt1bY* sex determination gene (Volff and Schartl, 2002, Matsuda et al., 2002) and the well-known *foxl3* (Forkhead box L3), the female germline sex determinator (Nishimura et al., 2015, Kikuchi et al., 2020), have made medaka fish a good experimental model for the study of germline proliferation and differentiation. Like most vertebrates, female germ cells in medaka enter oogenesis at hatching, while male germ cells continue in a state of mitotic arrest until they initiate spermatogenesis one month later in puberty medaka (Saito et al., 2007). XX germ cells are morphologically distinct from XY germ cells at 5 days post-hatching (dph) (Tanaka, 2019). The feminizing effect of germ cells has been demonstrated to be inherent and independent of somatic sex because the sex determination of germ cells occurs prior to the activation of the *dmy* master gene in somatic cells or the initiation of meiosis (Nishimura et al., 2018). The targeted disruption of gonadal soma-derived factor (*gsdf*), a unique BMP equivalent with a well-conserved transforming growth factor β (TGFβ) domain at its C-terminus, resulted in excessive germ cell proliferation and XY sexual reversal (Nishimura et al., 2018, Guan et al., 2017, Zhang et al., 2016, Imai et al., 2015). Nonetheless this XY feminization was suppressed in germ cell-deficient XY $gsdf^{-/-}$ lines (Nishimura et al., 2018), which is consistent with the requirement of germ cells in male-to-female sex-reversal. Transgenic over-expression of *gsdf* produced XX males in medaka (Zhang et al., 2016, Myosho et al., 2012), while *gsdf* mutants developed hypertrophic XY testes in both HdrR (*O. latipes*) and HNI (*Oryzias sakaizumii*) medaka (Zhang et al., 2021). All of these findings indicate that *gsdf* affects the sex-specific proliferation of XX and XY germ cells rather than the initiation of spermatogenesis (Zhang et al., 2021). The Gsdf signal may affect the proliferation rate of XX and XY germ cells, or the rate of cyst formation and subsequent cyst rupture. However, the underlying mechanism remains to be determined.

Incorporation of the thymidine analog 5'-ethynyl-2'-deoxyuridine (EdU) into chromosomal DNA is a simple method used to identify the DNA synthesis and chromatin architecture at the S-phase during cell proliferation. EdU has been reported to visualize germline division progress in *Caenorhabditis elegans* (Kocsisova et al., 2018). To decipher the Gsdf regulatory mechanism of sexual cyst formation *in vivo*, molecular differences between normal *gsdf*-intact and abnormal *gsdf*-deficient gametogenesis were characterized by RNA-sequencing and cytogenetic analyses. EdU incorporation was used to identify the sex differences in proliferating germ cells in the S phase of pre-meiotic proliferation in *gsdf*-deficient gonads, and details were further elucidated by immunofluorescent and transmission electron microscope (TEM) observations. The consequent quality of *gsdf*-deficient gametes was evaluated by the fertilization and embryo development of the offspring of *gsdf*-deficient XY individuals mating with normal partners.

Materials And Methods

Fish and mating schemes

Normal and *gsdf*-knockout medaka fish were housed in re-circulating systems at 26°C–28°C with a light-dark cycle of 14 h daylight and 10 h darkness. All the experimental procedures used in this study were approved by the Committee for Laboratory Animal Research of Shanghai Ocean University. Phenotypic sex and genotypic sex (XX or XY) were assessed following the previously reported protocol (Matsuda et al., 2002). Genotyping of the *gsdf* allele was performed with primers as described previously (Zhang et al., 2016). The mating schemes were as follows: $gsdf^{-/-}$ XY males (n = 3) paired with normal XX females (n = 3), $gsdf^{-/-}$ XY females (n = 4) paired with *gsdf*-transgenic XX males (n = 6), and $gsdf^{-/-}$ XX females (n = 3) paired with *Sissy* (a transgenic intersex line previously reported as Tg:cryG $gsdf^{-/-}$ XY males, n = 3) (Zhang et al., 2021). The results of breeding experiments are summarized in Table 1. All offspring from 11 mating families were raised to 3-month-old adulthood for genetic sex and phenotypic sex assessment. In the progeny analysis of Family 7 ($gsdf^{-/-}$ XY females paired with *gsdf*-transgenic XX males), *dmy* genotyping was carried out using embryos at stage 30.

Histological and ultrastructural observation

The protocol used for the histological section for hematoxylin and eosin (HE) staining was as previously described (Sun et al., 2017), and the results were viewed and photographed under the Nikon Ds-Ri2 (Nikon, Tokyo, Japan) or a confocal laser scanning microscope (DMi8 TCS SP8, Leica, Frankfurt, Germany). Ultrathin sections (70 nm thick) were prepared following a previously described method (Zhang et al., 2021) and examined with a FEI Tecnai G2 Spirit TEM (Thermo Fisher, Carlsbad, USA) at an acceleration voltage of 30 kV.

Identification of proliferative germ cells by EdU incorporation

Normal and *gsdf*-deficient gonads were subjected to EdU (RIBOBio, Guangzhou, China) staining for the identification of proliferating germ cells. Briefly, gonads of 3-month-old mature adults were added to EdU solution (20 μg/ml), incubated for 4 h at 28°C, fixed with 4% paraformaldehyde (PFA), and then embedded in paraffin (Shenggong Co., Ltd., Shanghai, China) after being dehydrated in a graded ethanol series. Cross-sections were cut at 5 μm thickness, then rehydrated and labeled with microfluorescence for 30 min incubation with fresh EdU cocktail (1xApollo dyeing reaction solution) according to the manufacturer's instructions (RIBOBio, Guangzhou, China), and then nuclei were counter-stained with 4',6-diamidino-2-phenylindole (DAPI). Apollo dye and DAPI fluorescent signals were photographed using a confocal laser scanning microscope (DMi8 TCS SP8, Leica, Germany).

Preparation of meiotic nuclear spreads and immunostaining

Germ cells were freshly collected by cutting adult gonads into small chunks. Cells were arrested by serum-free Dulbecco's Modified Eagle Medium (Gibco DMEM, Sigma-Aldrich, USA) in addition to

colchicines (10 ng/μm, Sigma-Aldrich, USA) prior to hypotonic 75 mM KCl treatment, and then fixed in Carnoy fix solution (3:1 methanol:acetic acid). Meiotic nuclear spreads were applied to clean slides and air dried. Slides were kept under − 20°C until use. Meiotic nuclear spreads were analyzed by Giemsa staining (Shenggong Co., Ltd., Shanghai, China), or incubated with primary antibodies and secondary antibodies (listed in Table S7) for immunofluorescence assay according to a previous report (Wu et al., 2019), and photographed with a Nikon Ds-Ri2 system (Nikon, Japan). All experiments were repeated at least three times with 3–5 individual fish.

Transcriptomic analysis

Total RNA was extracted from one-month-old puberty gonads of normal *gsdf*$^{+/+}$ testes (WTT) and ovaries (WTO), or *gsdf*$^{-/-}$ testes (HmT) and ovaries (HmO). The gonads of 7–15 individuals from each group were collected and pooled to minimize the impact of individual differences according to our previous report (Zhang et al., 2021). RNAs were cDNA reverse sequenced as 2x100-bp paired-end reads on the HiSeq 2000 platform (Illumina) by Shenggong Biotech Co., Ltd. (Shanghai, China). Clean reads were mapped to the medaka genome (http://www.ensembl.org/index.html) using the Reads Mapper Tophat2 (version 2.0.13, http://ccb.jhu.edu/software/tophat/). Sequence alignment and assembly were conducted using Cufflinks (version 2.2.0, http://cole-trapnell-lab.github.io/cufflinks/cufflinks/) and Cuffmerge (http://cole-trapnell-lab.github.io/cufflinks/cuffmerge/) software, and assemblies were merged into a master transcriptome for the analysis of differentially expressed genes (DEGs). A Venn diagram was plotted against the reads of unigenes across samples. A cut-off of false discovery rate (FDR) < 0.1 (Benjamini-Hochberg method) was used for MA-plot comparisons. The Integrative Genomics Viewer (IGV) was used to view RNA-Seq read coverage across the entire Japanese medaka HdrR viral genome (Ensembl genome browser 104: Japanese medaka HdrR - Description). The reads in the IGV display an automatically generated coverage track that contains a histogram of read depth for each coordinate across the genome. RNA sequence data have been deposited in the National Center for Biotechnology Information (NCBI) with the accession number PRJNA759752.

Structural prediction of Sycp1 and Sycp3 variants

The protein structures of full-length and splicing variants of wild-type Sycp1 and Sycp3 were predicted by the Phyre2 web portal through assessment under the ZDOCK server and visualization with the PyMOL molecular graphic system (www.sbg.ic.ac.uk/phyre2/html).

Statistical analysis

Statistics were analyzed and graphs were generated using the IBM SPSS statistics software for Windows version 26.0 (IBM Corporation, New York, NY, USA). An *ANOVA*-test was used to determine significant differences between normal and null animal measurements. P-values less than 0.05 were considered significant. Error bars represent the standard error of mean (SEM), unless otherwise noted.

Results

The differentially expressed genes regulated by Gsdf signaling

To identify the targeted genes responsible for Gsdf signaling before the initiation of spermatogenesis, RNA-seq was performed (transcriptome sequencing data were deposited in NCBI under accession number PRJNA759752).The differentially expressed genes (DEGs) were evaluated by comparing one-month-old *gsdf*$^{+/+}$ and *gsdf*$^{-/-}$ gonads before the XY germ cells resume proliferation (Saito et al., 2007, Kanamori, 1985), with the threshold of a $\log_2$ fold change (FC) ≥ 3 and a P-value of false discovery rate (FDR) < 0.05 as measures of statistical significance. FKB506-binding protein 7 (*fkbp7*), a molecular chaperone located in the endoplasmic reticulum (ER) as a suppressor of ATPase activity (Garrido et al., 2019), was remarkably upregulated ($\log_2$ FC ≥ 3), and overlapped among four pair-wise comparisons of normal testes to normal ovaries (WTT vs WTO); *gsdf*-deficient ovaries to normal ovaries (HmO vs WTO); *gsdf*-deficient testes to normal testes (HmT vs WTT); and *gsdf*-deficient testes to *gsdf*-deficient ovaries (HmT vs HmO) as revealed by Venn diagram (Fig. 1a). The details are listed in Table S1. RNA transcripts of follicle-stimulating hormone receptor (*fshr*), microRNA 202 (*miR202*), a zinc-finger protein with a C-terminal domain of four cysteine and two histidine residues (*zc4h2*), and an immunoglobulin-like domain factor were significantly upregulated in a subset of three comparisons: WTT vs WTO, HmO vs WTO, and HmT vs HmO.

To assess the concordance of RNA-seq data on expression quantification, the relative transcripts per kilobase expression of exon model per million mapped reads (mean TPMs) and $\log_2$MeanTPMs of sexually differentiated DEGs shown in Fig. 1b, were verified by real-time PCR quantification (qPCR) (Fig. 1c, details in Table S2 and Table S3). The sexually dimorphic expression of *fshr*, *sycp1*, *sycp3*, and *miR202* was consistent with previous reports (Gay et al., 2018, Aoki et al., 2009, Herpin et al., 2007), and was higher in the testis than in the ovary as verified by qPCR (Fig. 1C, Table S3), with primers listed in Table S4. The $\log_2$FC of *sycp3* (HmO vs WTO comparison) was 2.07, whereas that of *sycp1* (HmO vs WTO) was 4.3, indicating that the expression of *sycp1* was more sensitive to the Gsdf signal (Fig. 1b, Table S1). The expression of *sycp1* in the ovary was higher than that in the testis, resembling to the expression patterns of *dynll2* and *nanos3* (Fig. 1b). Nevertheless, the expression of *sycp1* increased significantly in one-month-old *gsdf*-intact and *gsdf*-deficient testes (Fig. 1c), indicating the high proportion of *sycp1*-expressing germ cells in testes before the initiation of spermatogenesis. The expression of *sycp3* was higher in normal or *gsdf*-deficient testes than in normal or *gsdf* deficient ovaries (Fig. 1b), resembling that of *fkbp7* and *dnaaf1* (dynein, axonemal, and assembly factor), and the structural maintenance of chromosome 1b (*smc1b*). *nanos2 and nanos3* are related to stem-cell-like characteristics and are differentially expressed in medaka germ cells (Aoki et al., 2009). Notably, an increase of *nanos3* was detected in both *gsdf* deficient ovaries and testes, compared to their normal counterpart gonads. In contrast to no difference between normal ovaries and *gsdf* deficient ovaries, *nanos2* expression significantly increased in *gsdf*-deficient testes compared to normal testes (Fig. 1c). These results showed that the population of *nanos2*-expressing germ cells were sensitive to Gsdf and

were mainly located in the testis, which was different from the population subsets of *nanos3*-expressing germ cells responsive to Gsdf in both the ovary and testis (Fig. 1c) (Zhang et al., 2021).

Meiotic recombination targeted by Gsdf signal

To assess the targeted transcriptomes and the related pathways responsive to Gsdf, Kyoto Encyclopedia of Genes and Genome (KEGG) enrichment analysis was performed to investigate common DEGs among three overlapped pair-wise comparisons (41 upregulated DEGs), or two overlapped pair-wise comparisons (44 downregulated DEGs), as revealed by Venn diagram (Fig. 1A). The KEGG-enriched pathways are displayed in Fig. 2A in a bubble map, while the full details are listed in Table S5. The peroxisome proliferator-activated receptor (PPAR) pathway is well characterized and activated by TGFβ signals (Pleniceanu et al., 2017). Glycerolipid metabolism, ECM-receptor interaction, cell adhesion molecules, and tight junction pathways were downregulated (Fig. 2A, right panel), which is consistent with the involvement of fatty acid synthesis in female-to-male sex reversal (Sakae et al., 2020). The pathway of DNA homologous recombination (HR) consisting of *sycp3* (localized in chromosome18, Chr18) and *sycp3 like* (*sycp3l*) (localized in chromosome11, chr11) was significantly upregulated (Fig. 1a and Fig. 2A) (Pasquier et al., 2016). RNA alternative splicing (AS) variants of *sycp3* lacking N-terminus transmembrane domains remarkably increased in *gsdf*-deficient gonads, which was confirmed by RT-PCR with primers flanking the region of *sycp3* exon 2 and 5' upstream adjacent *phka1a* (Fig. 2B, the right corner). The super-coil structure of normal Sycp3 was putatively replaced by the linear structure without N-terminus AS variants predicted by Phyre2 software (Fig. 2B, right). A high frequency of AS junction tracks was found in *sycp3l* and *sycp1* region as shown by IGV Sashimi plot. This suggests that the active splicing machinery may promote the translation of defective Sycp1 and Sycp3l proteins, thus further interfering with DNA repair and meiotic HR events.

Malformation of Balbiani body with abnormal expression of Sycp3-Piwi in gsdf deficient oocytes

Piwi, the major component of the meiotic nuage to silence the transposon activity during meiotic HR (Yashiro et al., 2018), was expressed predominantly in mitotic spermatogonia and oogonia as well as meiotic spermatocytes and oocytes, as shown by immunofluorescence analysis (Fig. 3). The anti-Sycp3 positive signals were detected in meiotic spermatocytes and oocytes (Fig. 3a–a'; Fig. 3b–b'). Strong anti-Sycp3 signals were detected in normal oocyte Balbiani bodis (Bbs), although they declined significantly in the small Bbs of *gsdf*-deficient XX and XY ovaries (Fig. 3c–c'; Fig. 3d–d'). The low level of Sycp3 protein may have been due to the blocked translation of defective *sycp3* itself as a variant or the instability of protein products in *gsdf* deficient oocytes (Fig. 3c-3d). Compared with normal oocytes (stage III oocytes in Fig. 3b), *gsdf* deficient oocytes have fewer Piwi nuages in the cytoplasm (stage III oocytes in Fig. 3d), suggesting that the special transposons may become active without being inhibited, thereby promoting DSBs or HR events in *gsdf*$^{-/-}$ oocytes.

Increase of HR errors in gsdf-deficient testes

Proliferative germ cells that undergo cyst-division are different between XY male and XX female (Saito et al., 2007), and are distinguishable by EdU (a thymidine analog) incorporation, while gonads without EdU treatment serve as a negative control (Figure S1). Although the spotted bars corresponding to chromosomes were obviously different between females (unevenly distributed in oogonia in Figure S2a_1–a_3) and males (evenly distributed in spermatogonia in Figure S2b_1–b_2), some spermatogonia were similar to oogonia in shape and pattern ($SpgB_{2a}$ in Figure S2b_2–b_2' vs Og in Figure S2a_3), but different from cystic spermatogonia ($SpgB_{2b}$ in Figure S2b_1'). The identical shape may have been derived from the same cell cycle stage, similar DSBs, or HR events shared by these germ cells. Like humans (Capalbo et al., 2017, Gruhn et al., 2013), medaka germ cells in normal spermatogenesis undergo HR errors occasionally (e.g., non-exchange chromosomes or achiasmate chromosomes) to become oocyte-like (Ol) cells (Figure S2c). The evidence of a large number of Ol cells in *Sissy* gonads supports the hypothesis that impaired Gsdf signaling leads to high-frequency HR errors during meiosis (Zhang et al., 2021).

The effect of Gsdf on meiosis was further investigated by EdU incorporation. According to the ratio of $SpgB_2$ per total SpgB number for three testes, each with 14 count fields EdU-positive, $SpgB_{2a}$ (ccOg alike) was double in *gsdf*-deficient testis (19.24%) compared to normal testis (10%) (Figure S3A–B). The counting results are summarized in Table S6. The separation of sister germ cells and cystic dividing cells are shown in Fig. 4.

Asynchronous cysts formation in gsdf-deficient testes

TEM observations showed that synchronous cysts containing cystic-proliferative spermatocytes (Spc) (Fig. 5a_1), spermatids (Spt) and sperm (Spm) (Fig. 5a_2), round and elongated spermatids (Fig. 5a_3- a_4), and densely packed sperm cells (Fig. 6a_5-6a_6) were present in the cross sections of normal testes (n = 3). However, many asynchronous cysts appeared in *gsdf* deficient XY testes, which showed that germ cells at different developmental stages were in the same cyst (Fig. 5b_1-b_4, n = 3) (Zhang et al., 2016). Spermatocytes (Spt), mitotic metaphase SpgB and sperm were present in a single cyst (Fig. 5b_1); dead Sertoli cells (*Sc) and ruptured cysts (Fig. 5b_2); round spermatids with loosened packaging of genomic DNA (Fig. 5b_3), and one cyst containing spermatozoa with irregular packaging of genomic DNA into tiny sperm heads (low magnification in Fig. 5b_4, and high magnification in Fig. 5$b_{4'}$-$b_{4''}$) were also found, supporting the theory that Piwi abnormality leads to the destruction of histone-protamine exchange during spermiogenesis (Gou et al., 2017).

Aneuploidy and low fertility of gsdf-deficient gametes

Meiosis in normal and gsdf deficient gametes was investigated using a cytological approach (Giemsa staining, Fig. 6). A total of 1312 prophase cells from normal and *gsdf*$^{-/-}$ testicular or ovarian biopsies were examined. The details are listed in Table S8. The defects were obvious as early as during the transition between leptotene/zygotene stages; instead of a bouquet configuration (Fig. 6a_{1-2}), loosened chromosome loops were observed in *gsdf*-deficient testes (arrows in Fig. 6a_3, enlarged in 6a_3') and ovaries (arrows in Fig. 6a_7–$a_{7'}$). Aneuploid chromosomes (n = 25) were found in *gsdf*-deficient

spermatocytes (Fig. 6a_4, a_5), in contrast to normal chromosomes in *gsdf*-intact XY spermatocytes (n = 24 shown in Fig. 6a_2). Incomplete synapsis formation may ultimately lead to pachytene prolongation and the failure of pachytene completion. The lack of Gsdf destroys the proportion of normal prophase stages through the early leptotene/zygotene transition, and prolongs the pachytene of *gsdf*$^{-/-}$ testis and ovary, suggesting that Gsdf may affect the initiation of meiosis and the formation of SC. The proportional distribution of prophase stages shown in Fig. 6A_8.

The qualities of *gsdf*$^{-/-}$ gametes were evaluated by breeding experiments. The fertilization rate of normal XY or transgenic *gsdf* XX sperm and normal XX oocytes ranged from 94.4–98.9% (Table 1, Family 9–12), whereas the fertilization rates of *gsdf* deficient sperm (Table 1, Family 1–3) and eggs (Table 1, Family 4–7) ranged from 56.6–71.9% and 41.7–76.4%, respectively. These results indicated that aneuploid chromosomes in *gsdf*-deficient gamete led to a serious decline in the fertility of oocyte and sperm. The fertilization rate of *gsdf*-deficient XX oocytes and *Sissy gsdf*$^{-/-}$ sperm were the lowest at 39.3% and 37.5%, respectively, as shown in Table 1 (Family 8). The embryogenesis was severely damaged and delayed from one-cell fertilization throughout the entirety of embryogenesis. Two-cell division was delayed and asymmetric, and embryo development was severely hindered (Fig. 6b–d). In contrast to normal embryos, which reached stage 18 (St18 late neurula stage, 26 h after fertilization) according to the embryogenesis stages (Iwamatsu, 2004), the offspring embryos of *gsdf*-deficient males and normal females were delayed in St13 (early and middle gastrula) (Fig. 6d). This result indicated that the embryogenesis was damaged at the beginning of development, which may affect the development of multiple tissues. To our surprise, progeny produced from mating families between *gsdf*-deficient XY males (n = 3) and normal XX females developed as all XY males, while the offspring of *gsdf*$^{-/-}$ XY females (n = 4) mated with *gsdf* transgenic XX males were XX, with seven males and 49 females derived from three mating families. Fry fish of Family 7 (*gsdf*-deficient XY female bred with Tg XX male) were dissected and *dmy*-genotyped at hatching and showed the ratio of four XY males to eight XX females (Table 1). These results suggest that XX and XY germ cells respond differently to Gsdf signaling. *gsdf*-deficient X-bearing oocytes and Y-bearing sperm have more survival advantages during the processes of oogenesis and spermatogenesis, respectively.

In summary, we describe the sex chromosomes susceptible to HR errors in *gsdf*$^{-/-}$ gametogenesis from the aspects of X-Y non-disjunction and aneuploidy abnormalities. The loss of *gsdf* leads to defective gametogenesis, stimulates FKBP7-mTOR activity and promotes female cytoskeleton assembly through the downstream robust mRNA transcripts and splicing variants. Nevertheless, *gsdf* deficiency does not block all male cascades. Aberrant expression of *sycp1* and *sycp3* eventually leads to mis-segregation between homologous chromosomes (Fig. 6a_3–$a_{3'}$), which is likely to result in the occurrence of aneuploidy gametes caused by the non-disjunction of X-Y chromosomes, This can also explain the low fertility of *gsdf*$^{-/-}$ gametes and the sex bias of *gsdf* deletion offspring.

Discussion

Germ cell proliferation is an energy-consuming and sexually dimorphic process. The discovery of the strong response of *fkbp7* expression to Gsdf signaling in this study, in addition to our previous report on the physical interaction between Gsdf and eukaryotic elongation factor 1α (eEF1α) (Zhang et al., 2021), suggests that Gsdf may directly or indirectly inhibit the *fkbp7*-mediated eEF1α–eIF4F eukaryotic mRNA translation machinery (Firczuk et al., 2013). Members of the FKBP family form rapamycin induced ternary complexes that inhibit mTOR-kinase activity, and affect microtubule stability via associated tau protein (Cioffi et al., 2011). They are also involved in protein folding, apoptosis, and transcription/translation balance. Co-localization of *Fkbp6* with *Sycp1* and *Sycp3* is required for the formation of the synaptonemal complex during meiotic prophase to allow the paired homologous chromosomes to cross over (Noguchi et al., 2008). Impairment of the above molecules will lead to abnormal chromosome pairing, which will further arrest these meiotic germ cells in the pachytene stage and remove them through apoptosis (Noguchi et al., 2008). As a meiotic monitor of the fidelity of homologous chromosome pairing in spermatogenesis (Crackower et al., 2003). *Fkbp6*$^{-/-}$ and *Sycp3*$^{-/-}$ mice displayed sex-specific differences in male and female fertility with male-specific infertility (Crackower et al., 2003, Ayarza et al., 2016). Although the physical binding or co-localization of medaka Fkbp7 and Sycp1/Sycp3 remains to be elucidated, the asynchronous cysts in *gsdf*-deficient testes, probably resulted from the incomplete meiosis of germ cells and progressive somatic cell apoptosis (Fig. 5). The activated splicing regulators, particularly small nuclear ribonucleoproteins (snRNPs) in *gsdf* deficiency (Zhang et al., 2021) may specifically escalate the pre-mRNA AS variants of *sycp3, sycp3l*, and *sycp1* (Fig. 2). However, the reduction of Sycp3 protein products resulted in the failure of the normal assembly framework of rigid SC (Fig. 2B), thereby resulting in synaptic instability and non-crossover DSBs, or the chromosomal mis-segregation found by cytological observations (Fig. 6a3-3'). This could further weaken the mechanical force to promote the mitosis-meiosis transition (Elkouby, 2017). The impairment of chromosome assembly and recombination by abnormal *sycp3* and *sycp1* in mice meiotic cells produced aneuploid gametes, whereas heterogenous germ cells were blocked at different stages, such as mitotic cessation and chromosomal desynapsis to the incomplete diplotene/embryonic stage (Ayarza et al., 2016). This occurred in *gsdf* deficient gametogenesis, as the cysts composed of differentiated germ cells were fused abnormally as the result of germ and somatic cell apoptosis in *gsdf*-deficient spermatogenesis (Fig. 7). In addition, heterogenous germ cells with positive or negative expression of Igf2bp3 and H3K27me3 coexisted in a single cyst of the *gsdf*$^{-/-}$ XY ovary (Wu et al., 2019).

The developmental arrest of primary oocytes in *gsdf*-deficient XY ovaries partially overlapped the phenotype of *fshr* and *miR202* disruption in medaka (Gay et al., 2018, Murozumi et al., 2014). However, the expression levels of *fshr* and *miR202* were significantly upregulated in *gsdf* deficient germ cells (Fig. 1). Human FSHR variants lacking exon 2 and/or exon 3 are unable to stimulate the FSH signaling cascade and are associated with subfertility in women (Karakaya et al., 2014). Alternative spliced variants of *fshr* may interfere with the development of *gsdf*-deficient oocytes, in addition to the canonical Smad3 dependent activation of *Fshr* promoter to increase the cell division rate of rat granulosa cells (Gong and McGee, 2009). In fact, the irreversible synergistic effect of TGFβ and FSH in the expression of *Fshr* mRNA, as demonstrated in cultured rat granulosa cells (Inoue et al., 2003), may explain the

prevalence of 100% ovotestis development in *Sissy* individuals (the line that restores the exogenous *gsdf* expression in endogenous *gsdf*-targeted disruption) (Zhang et al., 2021) by 10% compared to that of *hotei* (*amhr*2 mutant) (Morinaga et al., 2007).

Sycp1 has been demonstrated to be necessary for the complete pairing of homologs in meiosis of zebrafish meiosis (Imai et al., 2021). The large-scale replacement of the normal SCs by defective SCs may have been detected by meiotic checkpoints, thereby triggering apoptosis, as demonstrated in *Sycp3* and *Sycp1* knockout mice (Ayarza et al., 2016). Males form fewer DSBs than females, and sex-specific differences are noted in HR during human meiosis prior to the establishment of DSBs (Gruhn et al., 2013). Sex chromosomes are particularly susceptible to paternal meiotic errors (Hall et al., 2006), and the deduced aneuploid cells will be eliminated by checkpoint mechanisms acting either at pachytene, to eliminate cells with synaptic errors or at metaphase I to eliminate cells with univalent chromosomes (Hall et al., 2006). X and Y spermatozoa are produced at a 50:50 ratio during normal spermatogenesis according to Mendelian segregation, but this ratio is skewed by a set of differentiated expression proteins and genes, which has been reviewed (Rahman and Pang, 2019). It was noteworthy that *gsdf*-deficient XY germ cells produced a seriously skewed sex ratio in the offspring of three *gsdf*-deficient XY males mated with normal XX females, as well as *gsdf*-deficient XY females mated with *gsdf*-transgenic XX males, according to our previous report (Zhang et al., 2016). This finding suggests that *gsdf* is involved in monitoring the progression and maintaining the fidelity of homologous chromosome pairing in meiosis through the regulation of *sycp1* and *sycp3* transcription and splicing. However, oocytes adopt a synaptic configuration in which the single X chromosome ‘self pairs’ and thereby avoids detection. The effect of *gsdf* on the preferential survival of X-chromosomal oocytes and Y-chromosome sperm may provide some clues to explain why men with more brothers are more prone to have sons, while men with more sisters have a higher probability of having daughters (Taketo, 2015); this phenomenon may be due to ligand-receptor interaction and responsiveness, assuming that a common role is conserved between mammalian BMP/TGFβ function and medaka Gsdf.

In summary, our results suggest that Gsdf signaling is required for precise homologous chromosome pairing, recombination, and synapsis formation. through Sycp1–Sycp3 splicing variants in vertebrate pre-meiotic and meiotic differentiation. These mechanisms in *gsdf* deletion gametogenesis will help to elucidate the meiotic dysfunctions associated with infertility.

Declarations

Supplementary data

This is linked to the online version of the paper at XXX.

Declaration of competing interests

All authors declare that they have no conflicts of interest regarding the contents of this article.

Funding

This research did not receive any specific grant from any funding agency in the public, commercial or not-for-profit sector.

Author contribution statement

GuanG was the primary corresponding author and Liangbiao Chen was the secondary corresponding author, both designed the overall studies; GuanG, LiX, LiXW, LiW, GuoH, WangG, HuR, LiY, WangS, WuX and WangT performed methodological investigations; GuanG, LiX, LiXW, and LiW undertook writing and review; and GuanG, ChenL and ZhaoX performed funding acquisition and manuscript editing. All authors have read and approved the final manuscript.

Acknowledgments

This work was supported by the First Class Discipline Program for Fisheries from the Shanghai municipal government, a grant from the National Natural Science Foundation of China (81771545), the Guangdong Basic and Applied Basic Research Foundation (2020B1515020001), and a grant from the National Key Research and Development Program of China (2018YFD0900601). We also thank LetPub LLC (www.letpub.com) for language-editing services and NBRP medaka for providing the HdrR and HNI strains.

References

1. AOKI, Y., NAKAMURA, S., ISHIKAWA, Y. & TANAKA, M. 2009. Expression and syntenic analyses of four nanos genes in medaka. Zoolog Sci, 26, 112–8.
2. AYARZA, E., GONZALEZ, M., LOPEZ, F., FERNANDEZ-DONOSO, R., PAGE, J. & BERRIOS, S. 2016. Alterations in chromosomal synapses and DNA repair in apoptotic spermatocytes of Mus m. domesticus. Eur J Histochem, 60, 2677.
3. CAPALBO, A., HOFFMANN, E. R., CIMADOMO, D., UBALDI, F. M. & RIENZI, L. 2017. Human female meiosis revised: new insights into the mechanisms of chromosome segregation and aneuploidies from advanced genomics and time-lapse imaging. Hum Reprod Update, 23, 706–722.
4. CIOFFI, D. L., HUBLER, T. R. & SCAMMELL, J. G. 2011. Organization and function of the FKBP52 and FKBP51 genes. Curr Opin Pharmacol, 11, 308–13.
5. CRACKOWER, M. A., KOLAS, N. K., NOGUCHI, J., SARAO, R., KIKUCHI, K., KANEKO, H., KOBAYASHI, E., KAWAI, Y., KOZIERADZKI, I., LANDERS, R., MO, R., HUI, C. C., NIEVES, E., COHEN, P. E., OSBORNE, L. R., WADA, T., KUNIEDA, T., MOENS, P. B. & PENNINGER, J. M. 2003. Essential role of Fkbp6 in male fertility and homologous chromosome pairing in meiosis. Science, 300, 1291–5.
6. ELKOUBY, Y. M. 2017. All in one - integrating cell polarity, meiosis, mitosis and mechanical forces in early oocyte differentiation in vertebrates. Int J Dev Biol, 61, 179–193.

7. FIRCZUK, H., KANNAMBATH, S., PAHLE, J., CLAYDON, A., BEYNON, R., DUNCAN, J., WESTERHOFF, H., MENDES, P. & MCCARTHY, J. E. 2013. An in vivo control map for the eukaryotic mRNA translation machinery. Mol Syst Biol, 9, 635.
8. GARRIDO, M. F., MARTIN, N. J., BERTRAND, M., GAUDIN, C., COMMO, F., EL KALAANY, N., AL NAKOUZI, N., FAZLI, L., DEL NERY, E., CAMONIS, J., PEREZ, F., LERONDEL, S., LE PAPE, A., COMPAGNO, D., GLEAVE, M., LORIOT, Y., DESAUBRY, L., VAGNER, S., FIZAZI, K. & CHAUCHEREAU, A. 2019. Regulation of eIF4F Translation Initiation Complex by the Peptidyl Prolyl Isomerase FKBP7 in Taxane-resistant Prostate Cancer. *Clin Cancer Res*, 25, 710–723.
9. GAY, S., BUGEON, J., BOUCHAREB, A., HENRY, L., DELAHAYE, C., LEGEAI, F., MONTFORT, J., LE CAM, A., SIEGEL, A., BOBE, J. & THERMES, V. 2018. MiR-202 controls female fecundity by regulating medaka oogenesis. PLoS Genet, 14, e1007593.
10. GONG, X. & MCGEE, E. A. 2009. Smad3 is required for normal follicular follicle-stimulating hormone responsiveness in the mouse. Biol Reprod, 81, 730–8.
11. GOU, L. T., KANG, J. Y., DAI, P., WANG, X., LI, F., ZHAO, S., ZHANG, M., HUA, M. M., LU, Y., ZHU, Y., LI, Z., CHEN, H., WU, L. G., LI, D., FU, X. D., LI, J., SHI, H. J. & LIU, M. F. 2017. Ubiquitination-Deficient Mutations in Human Piwi Cause Male Infertility by Impairing Histone-to-Protamine Exchange during Spermiogenesis. Cell, 169, 1090–1104 e13.
12. GRUHN, J. R., RUBIO, C., BROMAN, K. W., HUNT, P. A. & HASSOLD, T. 2013. Cytological studies of human meiosis: sex-specific differences in recombination originate at, or prior to, establishment of double-strand breaks. PLoS One, 8, e85075.
13. GUAN, G., SUN, K., ZHANG, X., ZHAO, X., LI, M., YAN, Y., WANG, Y., CHEN, J., YI, M. & HONG, Y. 2017. Developmental tracing of oocyte development in gonadal soma-derived factor deficiency medaka (Oryzias latipes) using a transgenic approach. Mech Dev, 143, 53–61.
14. HALL, H., HUNT, P. & HASSOLD, T. 2006. Meiosis and sex chromosome aneuploidy: how meiotic errors cause aneuploidy; how aneuploidy causes meiotic errors. Curr Opin Genet Dev, 16, 323–9.
15. HERPIN, A., ROHR, S., RIEDEL, D., KLUEVER, N., RAZ, E. & SCHARTL, M. 2007. Specification of primordial germ cells in medaka (Oryzias latipes). BMC Dev Biol, 7, 3.
16. HUNT, P. A. & HASSOLD, T. J. 2002. Sex matters in meiosis. Science, 296, 2181–3.
17. IMAI, T., SAINO, K. & MATSUDA, M. 2015. Mutation of Gonadal soma-derived factor induces medaka XY gonads to undergo ovarian development. Biochem Biophys Res Commun, 467, 109–14.
18. IMAI, Y., SAITO, K., TAKEMOTO, K., VELILLA, F., KAWASAKI, T., ISHIGURO, K. I. & SAKAI, N. 2021. Sycp1 Is Not Required for Subtelomeric DNA Double-Strand Breaks but Is Required for Homologous Alignment in Zebrafish Spermatocytes. Front Cell Dev Biol, 9, 664377.
19. INOUE, K., NAKAMURA, K., ABE, K., HIRAKAWA, T., TSUCHIYA, M., OOMORI, Y., MATSUDA, H., MIYAMOTO, K. & MINEGISHI, T. 2003. Mechanisms of action of transforming growth factor beta on the expression of follicle-stimulating hormone receptor messenger ribonucleic acid levels in rat granulosa cells. Biol Reprod, 69, 1238–44.

20. IWAMATSU, T. 2004. Stages of normal development in the medaka Oryzias latipes. Mech Dev, 121, 605–18.
21. KANAMORI, A., NAGAHAMA, Y., EGAMI, N. 1985. Development of the tissue architecture in the gonads of the medaka Oryzias latipes. Zool Sci, 2, 695–706.
22. KARAKAYA, C., GUZELOGLU-KAYISLI, O., HOBBS, R. J., GERASIMOVA, T., UYAR, A., ERDEM, M., OKTEM, M., ERDEM, A., GUMUSLU, S., ERCAN, D., SAKKAS, D., COMIZZOLI, P., SELI, E. & LALIOTI, M. D. 2014. Follicle-stimulating hormone receptor (FSHR) alternative skipping of exon 2 or 3 affects ovarian response to FSH. Mol Hum Reprod, 20, 630–43.
23. KIKUCHI, M., NISHIMURA, T., ISHISHITA, S., MATSUDA, Y. & TANAKA, M. 2020. foxl3, a sexual switch in germ cells, initiates two independent molecular pathways for commitment to oogenesis in medaka. Proc Natl Acad Sci U S A, 117, 12174–12181.
24. KOCSISOVA, Z., MOHAMMAD, A., KORNFELD, K. & SCHEDL, T. 2018. Cell Cycle Analysis in the C. elegans Germline with the Thymidine Analog EdU. J Vis Exp.
25. MATSUDA, M., NAGAHAMA, Y., SHINOMIYA, A., SATO, T., MATSUDA, C., KOBAYASHI, T., MORREY, C. E., SHIBATA, N., ASAKAWA, S., SHIMIZU, N., HORI, H., HAMAGUCHI, S. & SAKAIZUMI, M. 2002. DMY is a Y-specific DM-domain gene required for male development in the medaka fish. *Nature*, 417, 559 – 63.
26. MIYAUCHI, H., OHTA, H., NAGAOKA, S., NAKAKI, F., SASAKI, K., HAYASHI, K., YABUTA, Y., NAKAMURA, T., YAMAMOTO, T. & SAITOU, M. 2017. Bone morphogenetic protein and retinoic acid synergistically specify female germ-cell fate in mice. EMBO J, 36, 3100–3119.
27. MORINAGA, C., SAITO, D., NAKAMURA, S., SASAKI, T., ASAKAWA, S., SHIMIZU, N., MITANI, H., FURUTANI-SEIKI, M., TANAKA, M. & KONDOH, H. 2007. The hotei mutation of medaka in the anti-Mullerian hormone receptor causes the dysregulation of germ cell and sexual development. Proc Natl Acad Sci U S A, 104, 9691–6.
28. MUROZUMI, N., NAKASHIMA, R., HIRAI, T., KAMEI, Y., ISHIKAWA-FUJIWARA, T., TODO, T. & KITANO, T. 2014. Loss of follicle-stimulating hormone receptor function causes masculinization and suppression of ovarian development in genetically female medaka. Endocrinology, 155, 3136–45.
29. MYOSHO, T., OTAKE, H., MASUYAMA, H., MATSUDA, M., KUROKI, Y., FUJIYAMA, A., NARUSE, K., HAMAGUCHI, S. & SAKAIZUMI, M. 2012. Tracing the emergence of a novel sex-determining gene in medaka, Oryzias luzonensis. *Genetics*, 191, 163 – 70.
30. NISHIMURA, T., SATO, T., YAMAMOTO, Y., WATAKABE, I., OHKAWA, Y., SUYAMA, M., KOBAYASHI, S. & TANAKA, M. 2015. Sex determination. foxl3 is a germ cell-intrinsic factor involved in sperm-egg fate decision in medaka. Science, 349, 328–31.
31. NISHIMURA, T. & TANAKA, M. 2016. The Mechanism of Germline Sex Determination in Vertebrates. Biol Reprod, 95, 30.
32. NISHIMURA, T., YAMADA, K., FUJIMORI, C., KIKUCHI, M., KAWASAKI, T., SIEGFRIED, K. R., SAKAI, N. & TANAKA, M. 2018. Germ cells in the teleost fish medaka have an inherent feminizing effect. PLoS Genet, 14, e1007259.

33. NOGUCHI, J., OZAWA, M., NAKAI, M., SOMFAI, T., KIKUCHI, K., KANEKO, H. & KUNIEDA, T. 2008. Affected homologous chromosome pairing and phosphorylation of testis specific histone, H2AX, in male meiosis under FKBP6 deficiency. J Reprod Dev, 54, 203–7.
34. PASQUIER, J., CABAU, C., NGUYEN, T., JOUANNO, E., SEVERAC, D., BRAASCH, I., JOURNOT, L., PONTAROTTI, P., KLOPP, C., POSTLETHWAIT, J. H., GUIGUEN, Y. & BOBE, J. 2016. Gene evolution and gene expression after whole genome duplication in fish: the PhyloFish database. BMC Genomics, 17, 368.
35. PLENICEANU, O., SHUKRUN, R., OMER, D., VAX, E., KANTER, I., DZIEDZIC, K., PODE-SHAKKED, N., MARK-DANIEI, M., PRI-CHEN, S., GNATEK, Y., ALFANDARY, H., VARDA-BLOOM, N., BAR-LEV, D. D., BOLLAG, N., SHTAINFELD, R., ARMON, L., URBACH, A., KALISKY, T., NAGLER, A., HARARI-STEINBERG, O., ARBISER, J. L. & DEKEL, B. 2017. Peroxisome proliferator-activated receptor gamma (PPARgamma) is central to the initiation and propagation of human angiomyolipoma, suggesting its potential as a therapeutic target. EMBO Mol Med, 9, 1763.
36. RAHMAN, M. S. & PANG, M. G. 2019. New Biological Insights on X and Y Chromosome-Bearing Spermatozoa. Front Cell Dev Biol, 7, 388.
37. SADA, A., SUZUKI, A., SUZUKI, H. & SAGA, Y. 2009. The RNA-Binding Protein NANOS2 Is Required to Maintain Murine Spermatogonial Stem Cells. Science, 325, 1394–1398.
38. SAITO, D., MORINAGA, C., AOKI, Y., NAKAMURA, S., MITANI, H., FURUTANI-SEIKI, M., KONDOH, H. & TANAKA, M. 2007. Proliferation of germ cells during gonadal sex differentiation in medaka: Insights from germ cell-depleted mutant zenzai. Dev Biol, 310, 280–90.
39. SAKAE, Y., OIKAWA, A., SUGIURA, Y., MITA, M., NAKAMURA, S., NISHIMURA, T., SUEMATSU, M. & TANAKA, M. 2020. Starvation causes female-to-male sex reversal through lipid metabolism in the teleost fish, medaka (Olyzias latipes). Biol Open, 9.
40. SUN, K., FAN, L., WANG, C., YANG, X., ZHU, S., ZHANG, X., CHEN, X., HONG, Y. & GUAN, G. 2017. Loss of gonadal soma derived factor damaging the pituitary-gonadal axis in medaka. Science Bulliten, 62, 159–161.
41. TAKETO, T. 2015. The role of sex chromosomes in mammalian germ cell differentiation: can the germ cells carrying X and Y chromosomes differentiate into fertile oocytes? Asian J Androl, 17, 360–6.
42. TANAKA, M. 2019. Regulation of germ cell sex identity in medaka. Curr Top Dev Biol, 134, 151–165.
43. VERNET, N., DENNEFELD, C., KLOPFENSTEIN, M., RUIZ, A., BOK, D., GHYSELINCK, N. B. & MARK, M. 2008. Retinoid X receptor beta (RXRB) expression in Sertoli cells controls cholesterol homeostasis and spermiation. Reproduction, 136, 619–26.
44. VOLFF, J. N. & SCHARTL, M. 2002. Sex determination and sex chromosome evolution in the medaka, Oryzias latipes, and the platyfish, Xiphophorus maculatus. Cytogenet Genome Res, 99, 170–7.
45. WU, X., ZHANG, Y., XU, S., CHANG, Y., YE, Y., GUO, A., KANG, Y., GUO, H., XU, H., CHEN, L., ZHAO, X. & GUAN, G. 2019. Loss of Gsdf leads to a dysregulation of Igf2bp3-mediated oocyte development in medaka. Gen Comp Endocrinol, 277, 122–129.

46. YASHIRO, R., MUROTA, Y., NISHIDA, K. M., YAMASHIRO, H., FUJII, K., OGAI, A., YAMANAKA, S., NEGISHI, L., SIOMI, H. & SIOMI, M. C. 2018. Piwi Nuclear Localization and Its Regulatory Mechanism in Drosophila Ovarian Somatic Cells. Cell Rep, 23, 3647–3657.
47. ZHANG, X., CHANG, Y., ZHAI, W., QIAN, F., ZHANG, Y., XU, S., GUO, H., WANG, S., HU, R., ZHONG, X., ZHAO, X., CHEN, L. & GUAN, G. 2021. A Potential Role for the Gsdf-eEF1alpha Complex in Inhibiting Germ Cell Proliferation: A Protein-Interaction Analysis in Medaka (Oryzias latipes) From a Proteomics Perspective. Mol Cell Proteomics, 20, 100023.
48. ZHANG, X., GUAN, G., LI, M., ZHU, F., LIU, Q., NARUSE, K., HERPIN, A., NAGAHAMA, Y., LI, J. & HONG, Y. 2016. Autosomal gsdf acts as a male sex initiator in the fish medaka. Sci Rep, 6, 19738.

Table

Table 1 Genotypic and phenotypic analysis of progenies from mutant and normal lines

Types	Family	Fertilized eggs/total eggs	Hatching	3-month-old adults
		(Fertilization rate)	(Survival rate)	♂:♀
gsdf$^{-/-}$XY♂ x *gsdf*$^{+/+}$XX♀	1	82/145 (56.6%)	47/82 (57.3%)	15:0 (all XY)
	2	91/148 (61.5%)	35/91 (38.5%)	22: 0 (all XY)
	3	87/121 (71.9%)	32/87 (36.8%)	24: 0 (all XY)
gsdf$^{-/-}$XY♂ x *Tg: gsdf*$^{+/+}$XX♀	4	73/170 (42.9%)	38/73 (52.1%)	2:16 (all XX)
	5	87/127 (68.5%)	42/87 (48.3%)	4:22 (all XX)
	6	55/72 (76.4%)	28/55 (50.9%)	1:11 (all XX)
	7	30/72 (41.7%)	12/30 (40%)	(embryos St30 4XY:8XX)
gsdf$^{-/-}$XX♀ x *Sissy gsdf*$^{-/-}$XY♂	8	48/122 (39.3%)	18/48 (37.5%)	4XY:12 XX (SissyXY♂:XX♀)
gsdf$^{+/+}$XY♂ x *gsdf*$^{+/+}$XX♀	9	198/209 (94.7%)	179/198 (90.4%)	62:75 (XY♂:XX♀)
Tg: gsdf$^{+/+}$XX♀ x *gsdf*$^{+/+}$XX♀	10	205/212(96.7%)	186/205 (90.7%)	80:95 (XY♂:XX♀)
	11	170/180 (94.4%)	154/170 (90.6%)	28:114 (XX♂:XX♀)
	12	138/143 (98.9%)	122/138 (88.4%)	21:87 (XX♂:XX♀)

Figures

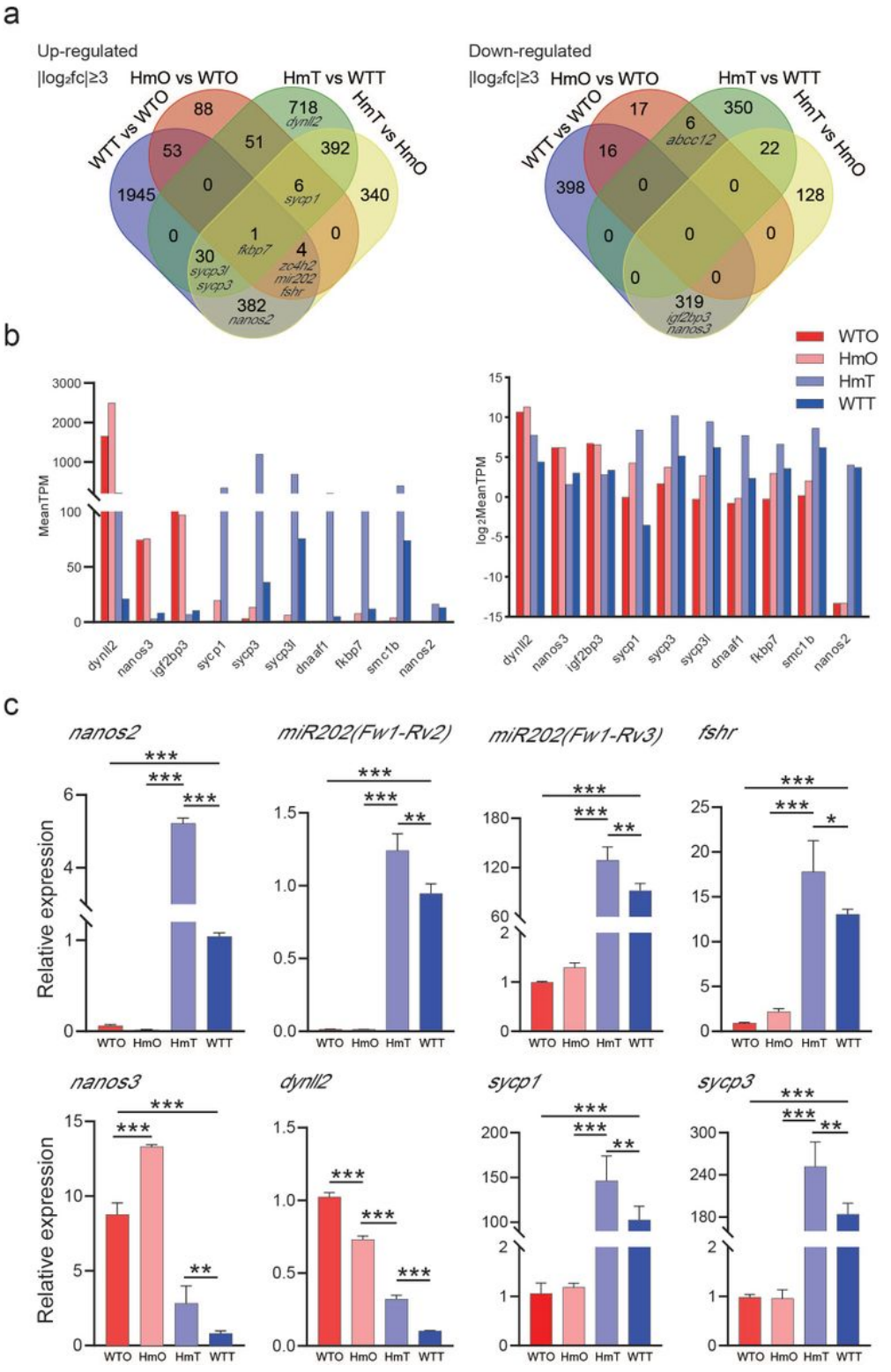

Figure 1

Comparative analysis of transcript abundance among *gsdf*-intact and -null gonads. (a) The Venn diagram shows the numbers of differentially expresseed genes (DEGs) in the upregulated or downregulated groups of four comparisons: normal ovaries (A, WTO) vs normal testes (B, WTT); A vs mutant ovaries (C, HmO); A vs mutant testes (D), C vs D. (b) The bar plot depicts the relative transcripts per kilobase expression of exon model per million mapped reads (TPM) in each comparison subset. (c)

mRNA TPM contents were verified by real-time PCR. All experiments were performed in triplicate. Vertical bars are the SEM. **, P<0.01; ***, P<0.001.

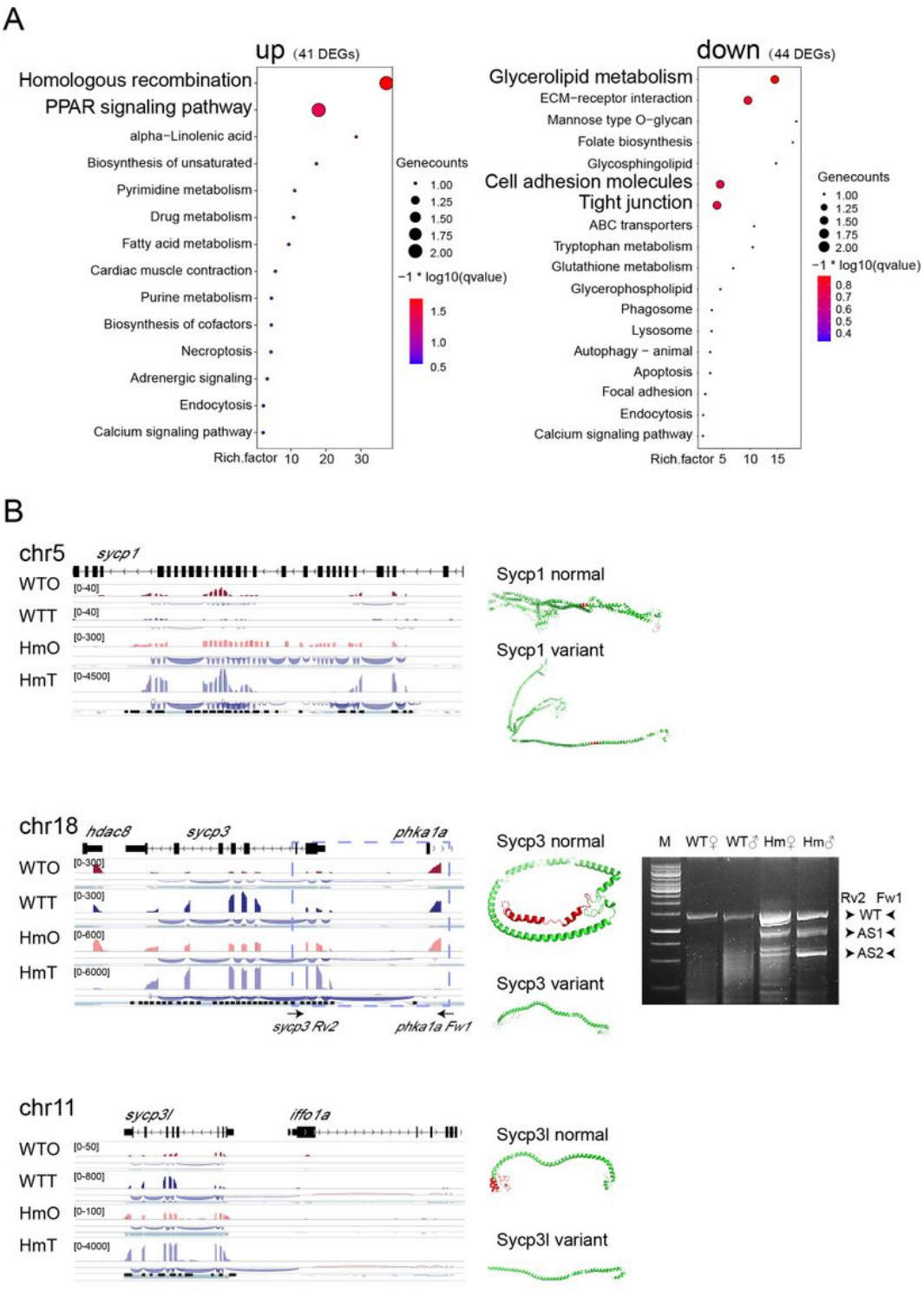

Figure 2

KEGG pathway and RNA splicing in *sycp3* (chr18) and *sycp3l* (chr11) *gsdf*-intact and -null gonads. (A) The bubble plot depicts the enriched KEGG pathways in upregulated and downregulated groups using a

novel R-based package, clusterProfiler. The bubble, with color ranging from red to blue, indicates a set of highly significant proteins. The diameter of the bubble indicates the number of genes related to the same KEGG pathway. (B) Integrative Genomics Viewer (IGV) visualization of the *sycp3* and *sycp3l* gene region. The RNA splicing variants were revealed by Sashimi plots and verified by RT-PCR (right corner in the middle).

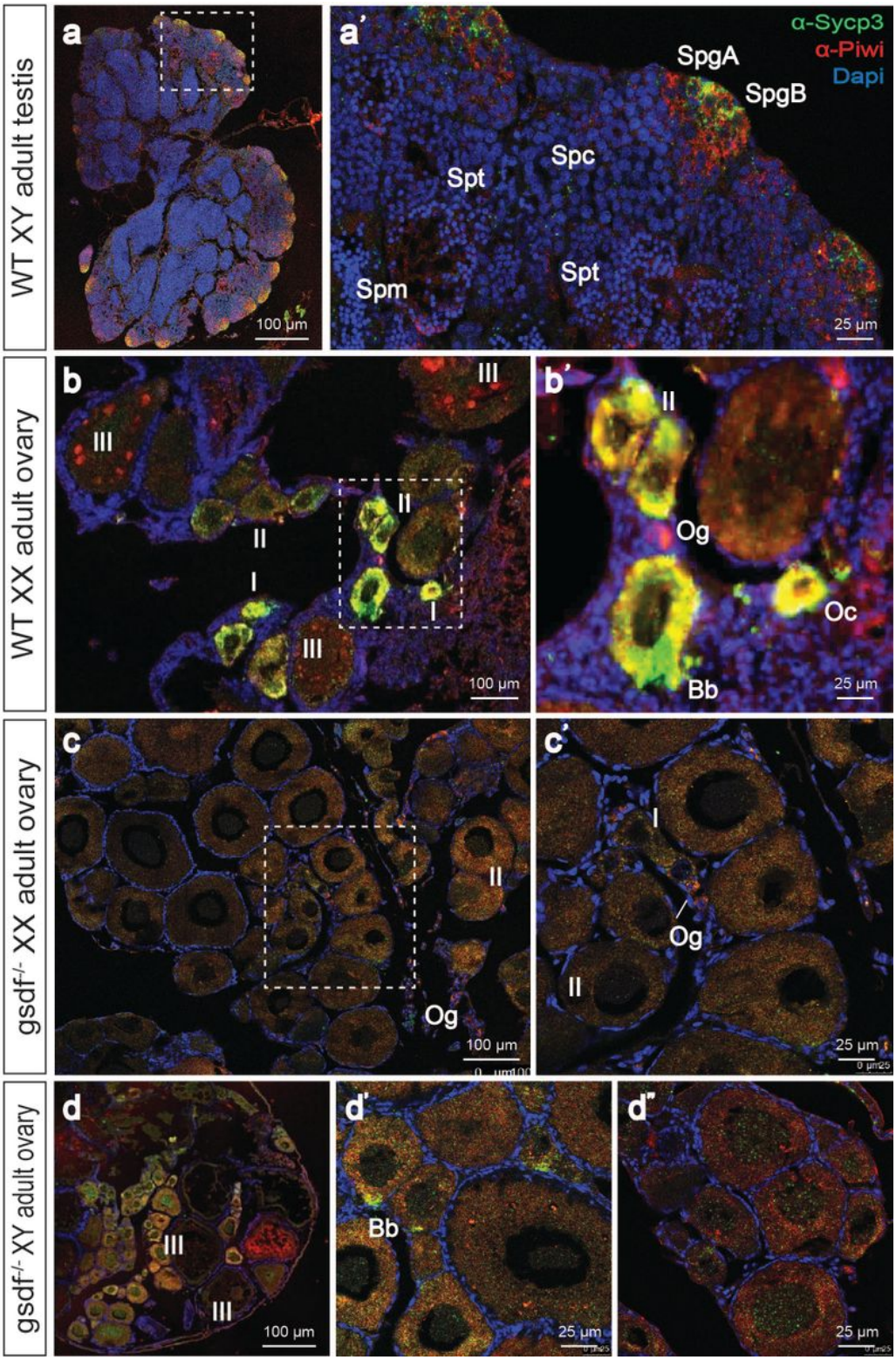

Figure 3

Defective Sycp3-Piwi expression and Balbinia body malformation in *gsdf* depletion oocytes. (a) Piwi is abundant in peripheral spermatogonia and spermatocytes in adult testis, (b) oogonia and subsequent stages of oocyte development in normal adult ovary. Unlike many Piwi positive particles in stage III oocytes in normal female, rare stage III oocytes were observed in gsdf depletion ovary (c-c', d-d'), with less particles. Scp3 expression in pre-leptotene spermatocytes towards pachytene spermatocyte, or stage I and II oocyte.

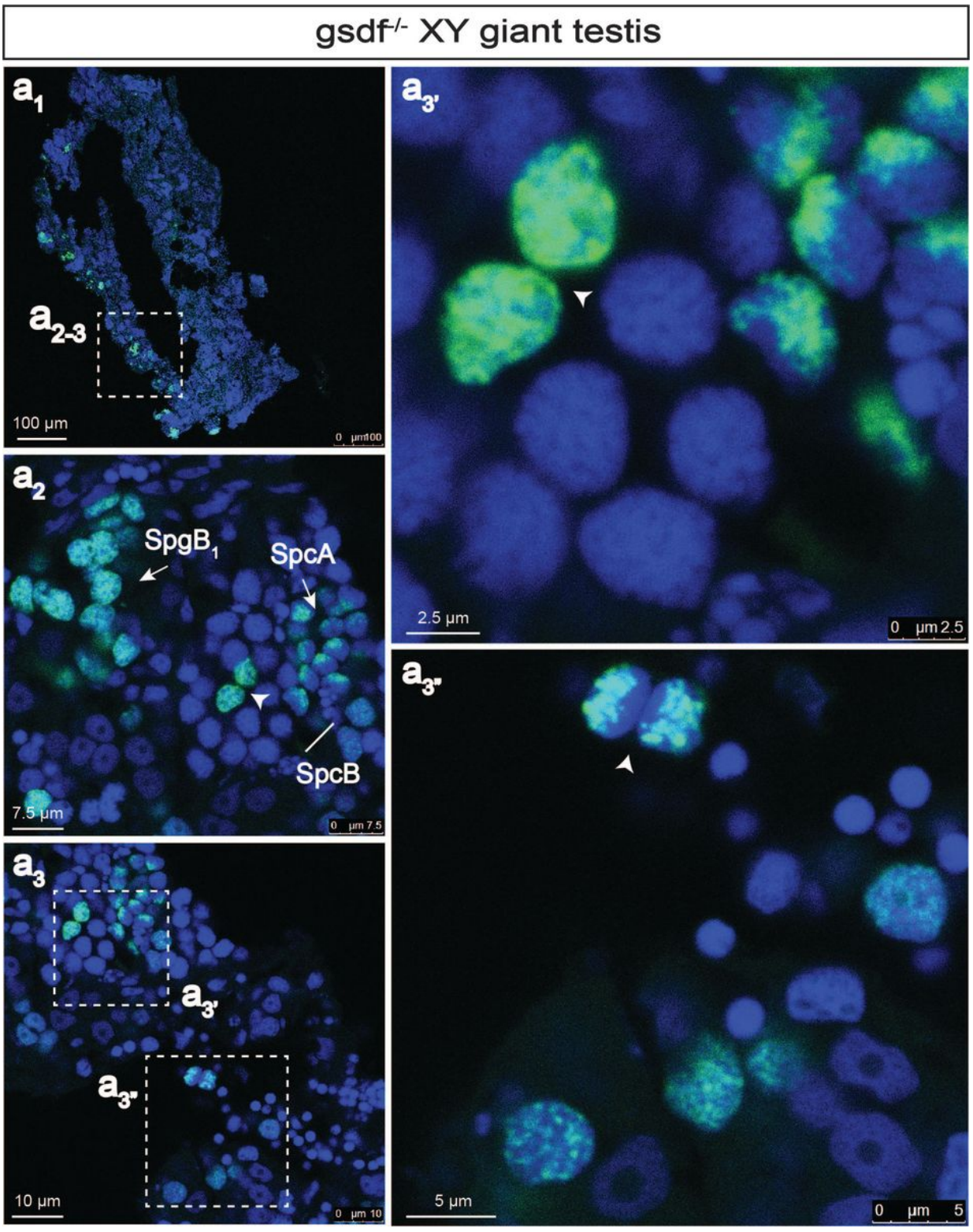

Figure 4

The specific proliferation of SpgB2a in *gsdf*-deficient testis. (a) Image of *gsdf*$^{-/-}$ XY testis under low magnification (a_1) and high magnification (a_2 and a_3; $a_{3'}$ and $a_{3''}$). The ratio of SpgB2a among total SpgB drastically increased in *gsdf*$^{-/-}$ testis, in contrast to the ratio of normal testis as a control shown in Figure S3, and details are listed in Table S3.

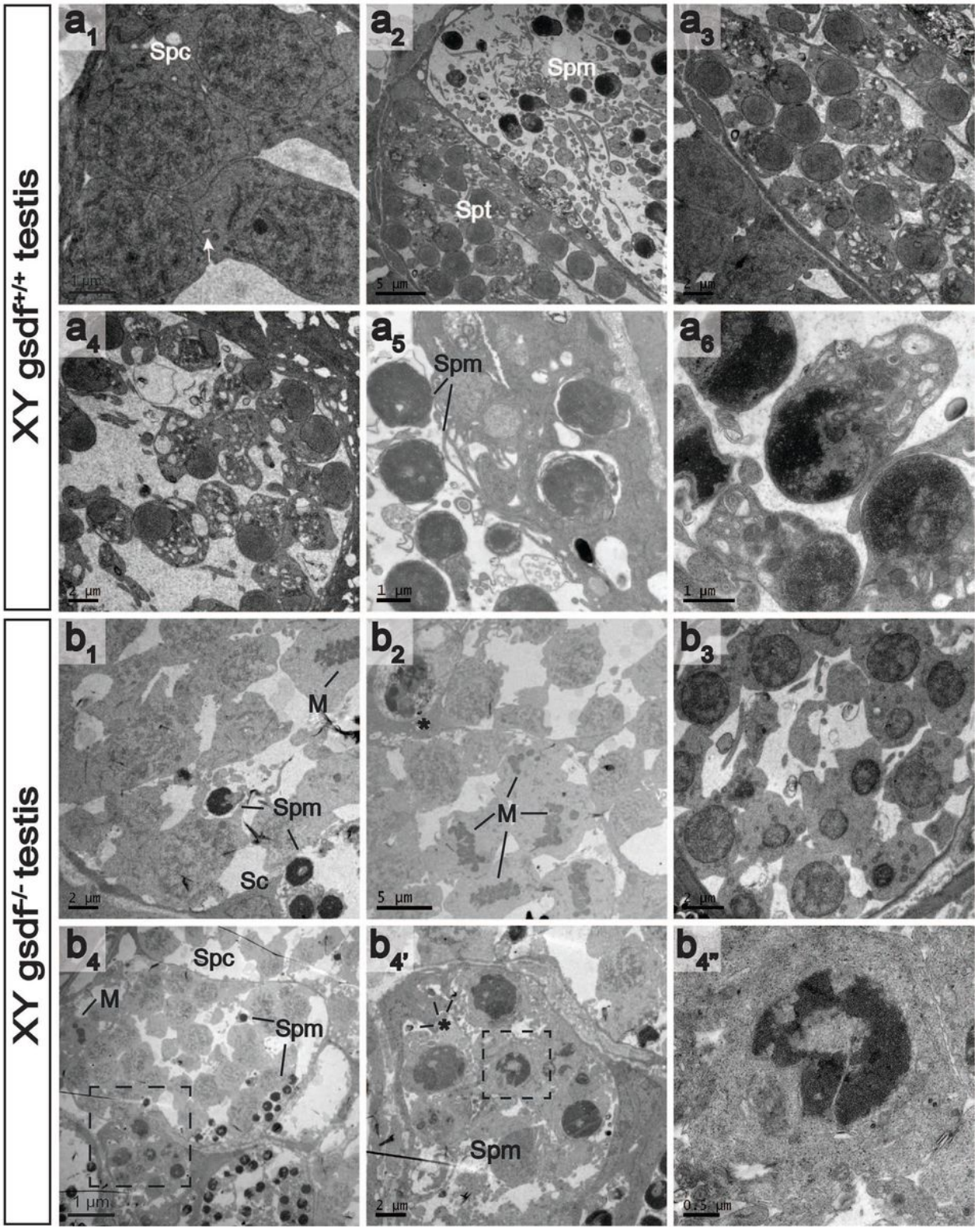

Figure 5

Ultrastructure of cysts in normal and *gsdf*-deficient testes. (a) Transmission electron microscope (TEM) ultrastructural images of various stages germ cells. Synchronous cysts in normal *gsdf*$^{+/+}$ spermatogenesis (a_1, spermatocytes) and asynchronous cysts in *gsdf*$^{-/-}$ testes (a_2, sperm) and (b_1, low magnification; b_2 high magnification). DC, distal centriole; PC, proximal centriole; Spg, spermatogia; Spc, spermatocyte; Spz: spermatozoa; Spt: spermatide; Spm: sperm.

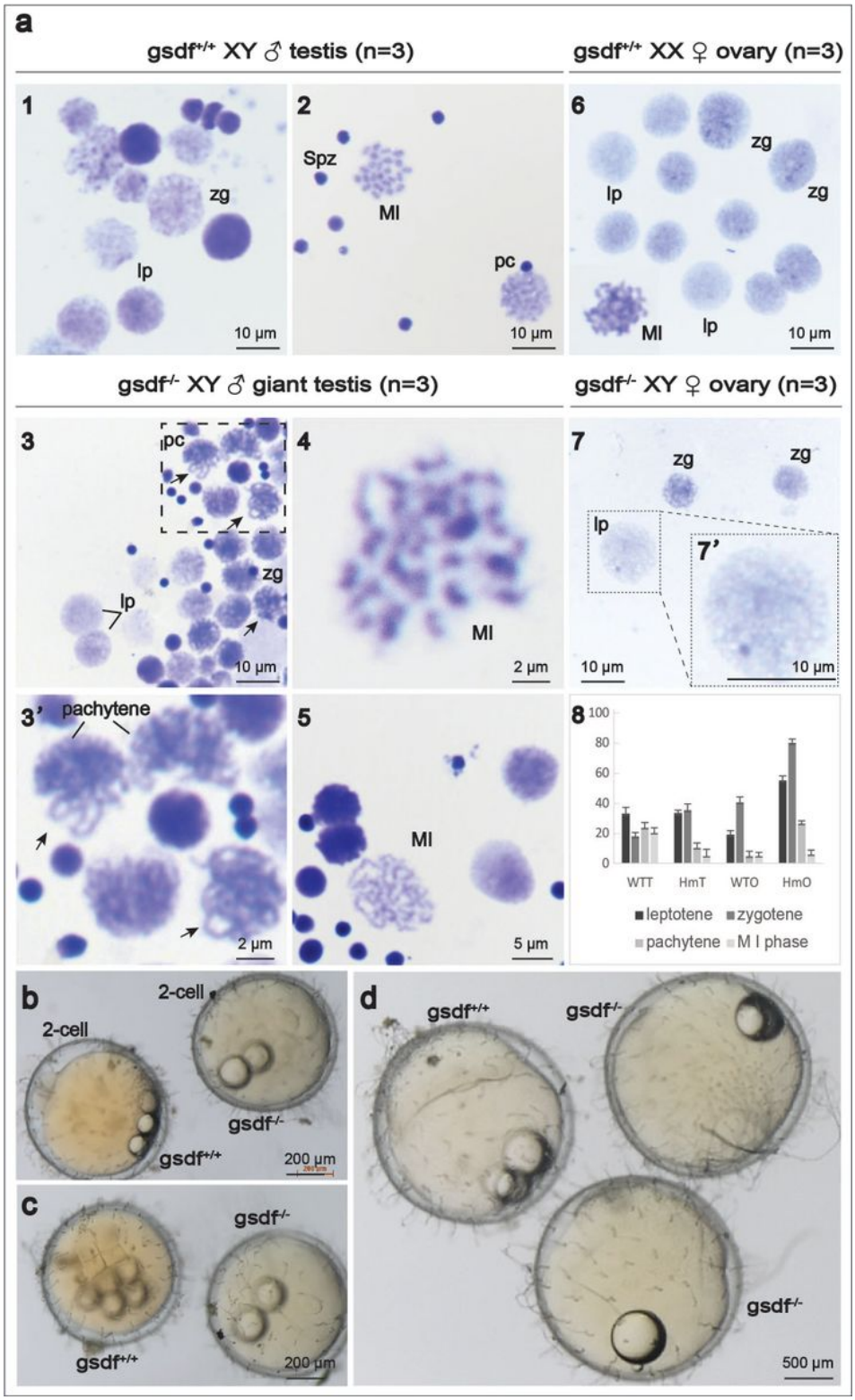

Figure 6

Representative meiosis spreads of intact and defective gsdf gonads. (a) Giemsa staining of normal (a1–2) and gsdf-null XY germ cells (a3, enlarged in a3', a4–5); normal (a6) and gsdf-deficient XX germ cells (a7–7'). The proportional distribution of normal and gsdf-deficient prophase stages (a8). Spg: spermatogonia, Spc: spermatocyte, Spz: spermatozoa. Embryogenesis defects were detectable as early as two-cell division (b), the four-cell stage (c), and throughout embryogenesis at neurula stage (d).

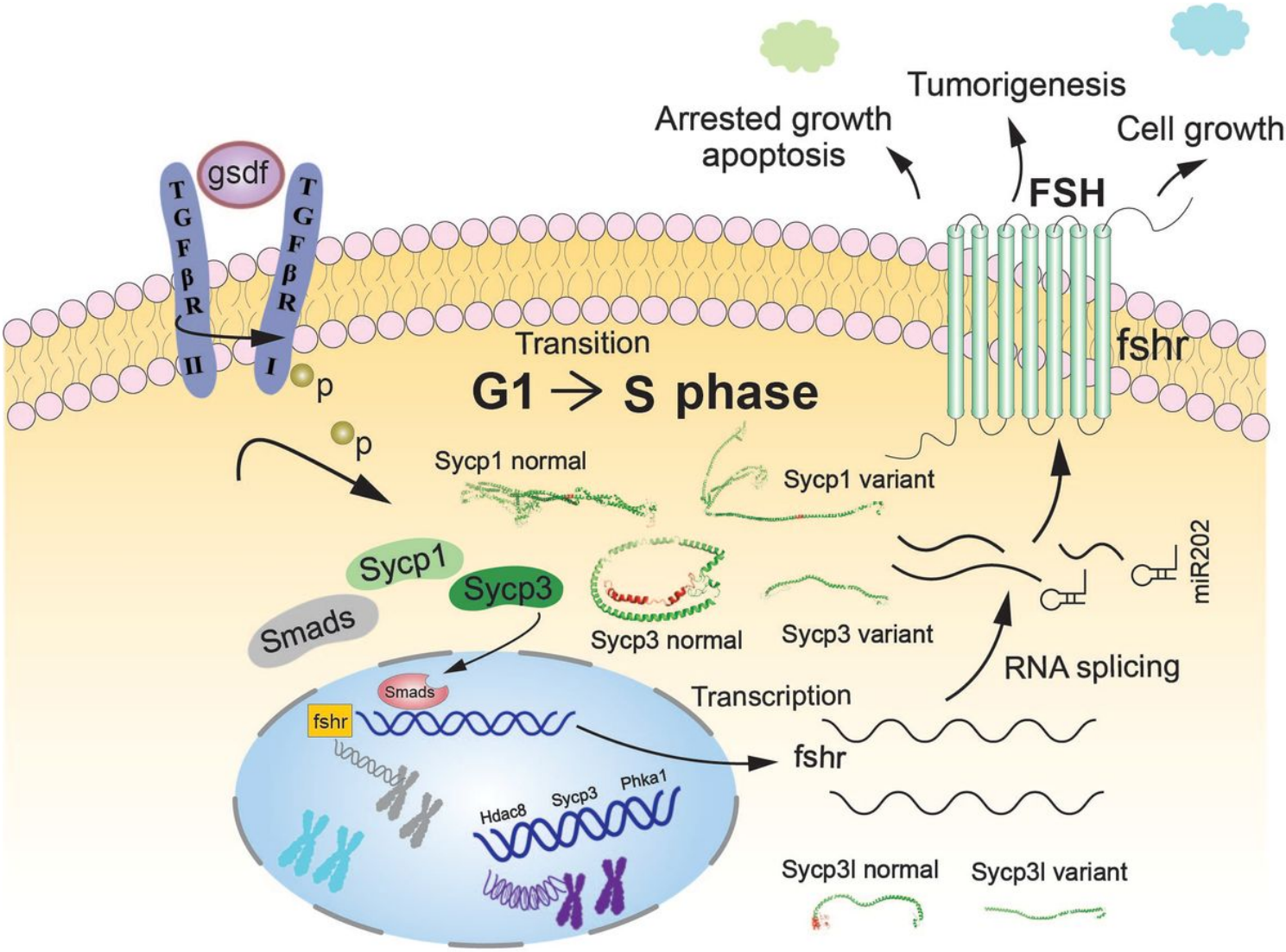

Figure 7

Schematic representation of the potential mechanisms of *gsdf* in XY gametogenesis. The hypothetical mechanisms of prolonged and delayed meiotic expansion in *gsdf*-deficient gametogenesis. In the process of mitotic proliferation and meiotic differentiation, Gsdf regulates *sycp1* and *sycp3* transcription and splicing to ensure correct chromosome pairing and segregation.

Supplementary Files

This is a list of supplementary files associated with this preprint. Click to download.

- SMCCS22.3.9.pdf
- SMFig.S1S3.pdf
- SMTableS1S8.pdf